Evidence of High-Temperature Strain Heterogeneities in a Nickel-Based Single-Crystal Superalloy

Damien Texier, Daniel Monceau, Ronan Mainguy, Eric Andrieu

Evidence of High-Temperature Strain Heterogeneities in a Nickel-Based Single-Crystal Superalloy**

By *Damien Texier, Daniel Monceau,* Ronan Mainguy* and *Eric Andrieu*

The use of single-crystal Ni-based superalloys is required in the manufacture of severely stressed structural parts such as high-pressure turbine blades.[1] Design calculations of such structural parts are based on data acquired from bulk specimens.[2] These results allow for the identification of constitutive laws that homogenize the microstructure response. The optimization of the macroscopic response of such materials is mostly due to studies on deformation mechanisms.[3,4] These studies show evidence of the fundamental role played by metallurgical states and particularly the major role played by the γ/γ' interface.[5–7] This type of approach generally conceives the biphasic γ/γ' material scale as billions of cuboidal or rafted γ'-$L1_2$ precipitates embedded in a fcc single crystal solid solution matrix. At the intermediate scale considered in the present study, the material is seen as a heterogeneous material composed of dendrites surrounded by interdendritic regions. The goal is to reveal, if they exist, differences in behavior between the dendritic zone (DZ) and interdendritic zone (IDZ). To this end, high-temperature creep experiments were carried out on specimens whose thicknesses were smaller than the periodicity of the dendritic pattern. Creep tests on specimens with micrometric thickness have already been performed under different atmospheres to highlight the impact of the environment on the mechanical properties of a turbine blade.[8–10] Indeed, great care must be taken to prevent any static or dynamic effect of oxidation on the mechanical behavior of specimens. Hence, the experiments reported in the present study were conducted under an atmosphere optimized for the exclusive growth of a very thin film of α-alumina at the surface of the specimens, without any major consequences on the mechanical behavior.[11]

[*] *D. Monceau, D. Texier, R. Mainguy, E. Andrieu*
CIRIMAT, ENSIACET-INPT, 4, Allée Emile Monso – BP 44362 F-31030, Toulouse, Cedex 4, France
E-mail: daniel.monceau@ensiacet.fr

[**] *The authors are particularly grateful to Turbomeca–SAFRAN group for providing the base material. This work was part of a research program supported by DGA involving Snecma-SAFRAN group, Turbomeca-SAFRAN, ONERA, CEAT, and CNRS laboratories (Mines Paris Tech, Institut P'-ENSMA, LMT-Cachan, LMS-X, CIRIMAT-ENSIACET). D. Texier is also grateful to B. Viguier, S. Dryepondt, P. Caron and J. Cormier for stimulating discussions. P. DeParseval and V. Baylac are thanked for their help with EPMA and interferometry analyses.*

The material used in this study is a first-generation superalloy MC2 with the following nominal composition, Ni–8.0Cr–5.0Co–2.0Mo–7.8W–5.0A1–1.5Ti–6.1Ta (wt%). A rod was solidified by a withdrawal process along the [001] crystallographic direction then submitted to a standard heat treatment (1300 °C-3 h + air cooling (A.C.) – 1080 °C-6 h + A.C. – 870 °C-20 h + A.C.). Due to the solidification settings, the dendritic pattern can be described as a nested arrangement. Despite the homogenizing heat treatment, the chemical segregation at the dendritic scale was large enough to be detected by scanning electronic microscopy (Figure 1). A mean distance of 330 μm between the primary dendrite axes (PDA) and 130 μm between secondary dendrite arms (SDA) was measured by image analysis.

Creep experiments were carried out with a device designed and developed specifically for the high-temperature mechanical characterization of ultrathin specimens under a controlled atmosphere. These tests were developed and optimized with the aim of defining operating conditions that prevent various problems from affecting the surfaces of the specimens, i.e., oxidation, nitridation, or sublimation. First-generation single-crystal superalloys are prone to be non-exclusive alumino-former alloys. Despite the steady-state formation of a continuous internal α-alumina layer, other oxides such as transition alumina oxides, spinels, or nickel oxide can grow on the sides or on top of the α-alumina layer.[12] At atmospheric pressure, even if an α-alumina layer grows much more slowly than other oxides, it can be shown that this surface degradation can still be detrimental to creep experiments on ultrathin samples. On the other hand, experiments under high vacuum favor the sublimation of the samples, which considerably affect the creep results. Ultimately, the best choice was to use a 1.2 bar Ar atmosphere combined with an O_2 getter (Zr flakes). This was shown to prevent metal sublimation and to limit alumina growth. SEM observations of cross sections of creep-tested samples allowed for the evaluation of the impact of alumina growth on the evolution of the samples' biphasic microstructure. Samples held for 40 h at 1100 °C did not exhibit any γ'-precipitate-free zone or modification of the chemical composition of the substrate.

The normalized concentration values (wt%) of segregating elements W, Ti and Ta are reported in the grayscale map shown in Figure 2. The darkest zones correspond to the highest concentration values. The dendritic motif clearly appears throughout the different elemental maps. The segregation coefficient for each element (K_i) was calculated from the EPMA

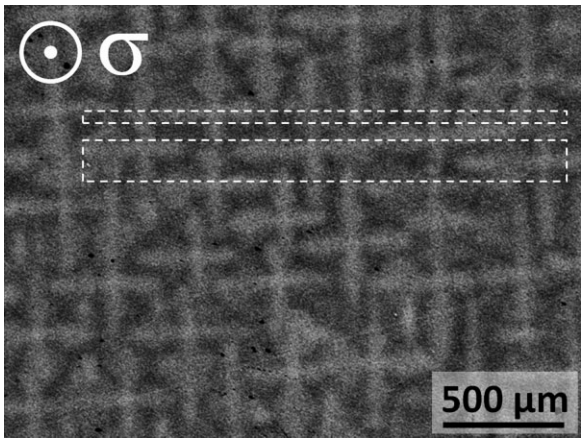

Fig. 1. Dendritic pattern normal to the loading axis. σ Arrow is the loading direction, rectangles are the 50 and 170 µm thick specimens after thinning down.

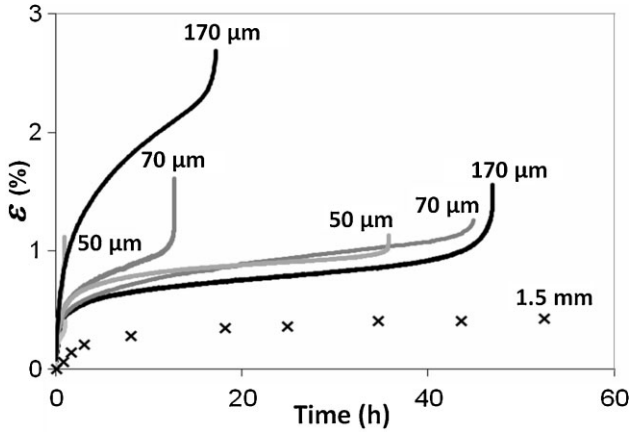

Fig. 3. Creep strain as a function of time for different specimen thicknesses of single-crystal superalloy at 1100 °C and an applied load of 100 MPa.

data, in accordance with the method used to quantify the level of segregation for "as-cast" alloys.[13,14] This parameter corresponds to the ratio between the mean values of the composition (in wt%) in the dendrite core and in the interdendritic region. Ni ($K_{Ni} = 0.98$), Ta ($K_{Ta} = 0.88$), and Ti ($K_{Ti} = 0.91$) were observed to segregate into the interdendritic region, unlike W ($K_W = 1.25$), which segregated into dendrite cores and secondary arms. Despite the fact that the K_i values are notably closer to 1 than the "as-cast" K_i values, these element distributions agree with those reported in previous studies.[15,16] The potential effect of the distribution of these alloying elements on the creep behavior and the thermal stability of the specimens' microstructure at high temperature justifies the choice to focus on the mesoscopic scale in this study.

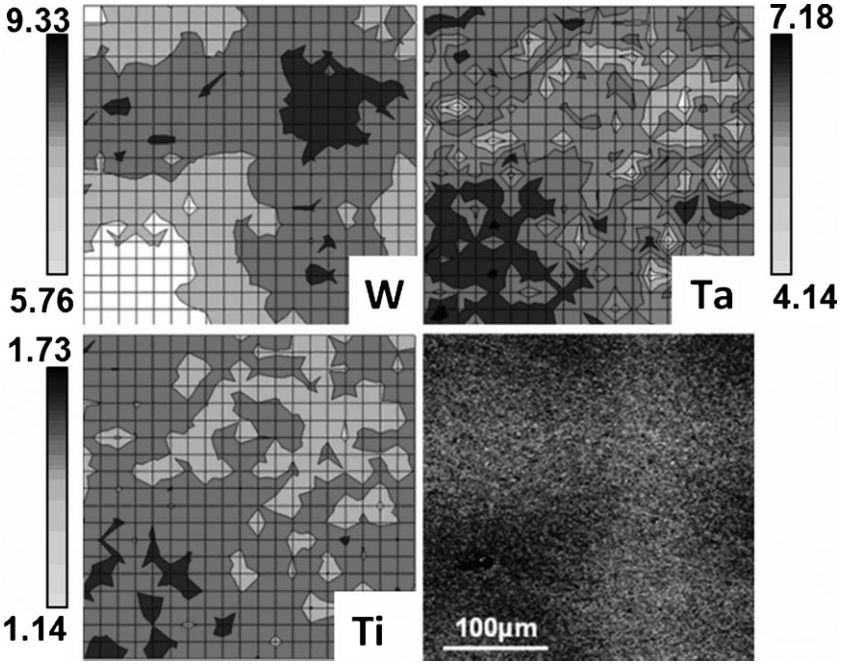

Fig. 2. Alloying element distribution at the dendrite scale (EPMA).

Creep experiments (1100 °C-100 MPa) were carried out on specimens with different thicknesses. The creep results demonstrate a high level of scattering (Figure 3). This dispersion is significantly higher than the dispersion expected from thickness irregularities or the uncertainty in the applied load (≈30%). The steady-state strain rates that were measured vary by two orders of magnitude, from 5.9×10^{-5} to $5.7 \times 10^{-3}\,h^{-1}$, and no direct correlation could be established between the sample thickness and the creep rate. BSE-SEM observations of specimens' surfaces show difference in proportion of dendritic and interdendritic area from a specimen to another one. Due to the thickness of specimen smaller than the dendritic pattern, the number of primary dendrite axes can be estimated and correlated to the value of steady state rates. Using the analogy of a composite material, considering the primary dendrite axes as long fibers and interdendritic region as the matrix, the more there are fibers in the section of the sample, smaller is the value of steady state rates. Hence, for a same level of stress applied, the value of the steady state rate evolves as a power law expression regarding to the number of dendrite cores, as reported in the Eq. (1).

$$\dot{\varepsilon} = K N_{PDA}^{n}, \quad \text{with } n = -5.7 \text{ and } K = 5.5\,h^{-1} \tag{1}$$

Under such creep conditions, the testing of 1.5 mm thick specimens at 1100 °C-100 MPa in air led to creep strain rates that were 17–50 times lower that those observed in ultrathin specimens (dotted curve in Figure 3). The propensity of ultrathin specimens to be more sensitive to damage can be attributed to the analogy of long fibers for thick specimens and short fibers for ultrathin specimens. It can also be attributed to the number and size of defects initially present

in the material. The foundry porosity, unavoidable to the elaboration process, was found to have a deleterious effect on creep resistance.[17] Several foundry pores could be observed on the fracture surfaces of ultrathin specimens. Nevertheless, such porosities (formed during casting or after homogenization heat treatment) are located in interdendritic regions. These defects weaken the "matrix" relatively to the "fibers" at the mesoscopic scale. The density of pores in the section of specimens is proportional to the interdendritic region volume fraction, thus inversely proportional to the fraction of dendrite cores. Such a difference in DZ/IDZ behavior is hidden by the repeatability of the dendritic pattern for creep experiments on thick specimens. However, this consideration has to be taken into account when discussing the modeling of airfoil blade.

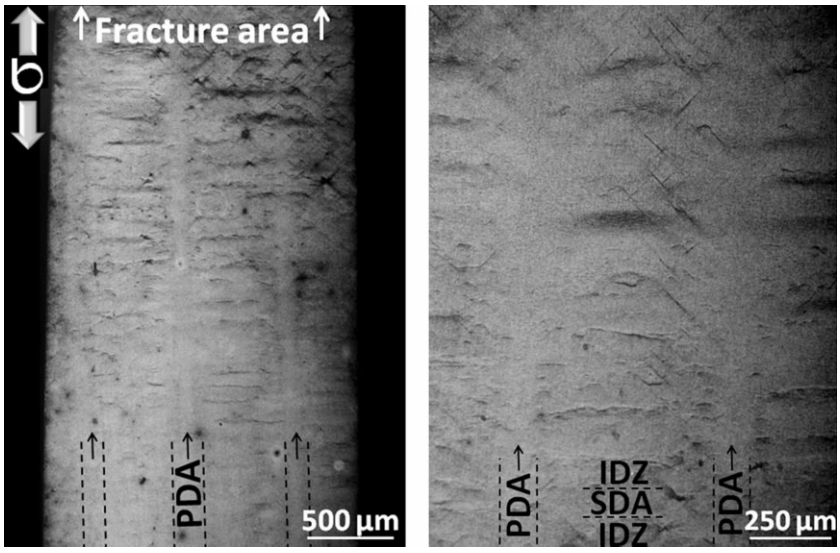

Fig. 4. Strain heterogeneity distribution observed on a creep-tested sample (optical microscopy): (a) LTD-LD observation of the entire width of the sample and (b) magnified image of area between two dendrite trunks.

The post-mortem topography of the sample gauge length surface was analyzed by optical microscopy and optical interferometer analyses to reveal, if they existed, strain heterogeneities. An additional creep experiment (1100 °C-140 MPa) was especially performed to conduct further surface observations. Optical microscopy observations of the surface showed that the variations in thickness were periodically distributed (Figure 4). These levels of roughness, which are indicative of the underlying microstructure, suggest heterogeneities in mechanical behavior between the dendrite core and the interdendritic region. The dotted lines in Figure 4 highlight three stripes with significantly lower roughness, corresponding to the PDA (BSE-SEM). Moreover, the surface deformation also seems to be periodically localized between these stripes whose period corresponds to the secondary dendrite arms (SDA) distance, i.e., approximately 130 µm.

The local topography of the specimen was investigated 2.5 mm away from the fracture area (Figure 5). The analyzed zone was also observed by BSE-SEM to correlate the level of roughness with the dendritic motif. The arithmetical roughness measured was minimal along the PDA ($Ra_{PDA} = 0.17$ µm) and maximal between them ($Ra_{SDA\text{-}IZ} = 0.62$ µm). Using the height of the primary dendrite axis as a reference, areas showing valleys and peaks correspond, respectively, to the interdendritic regions and SDA.

Such amplitude of the peak-to-valley variation is too high to be attributed solely to differences in the thermal expansion coefficient between DZ/IDZ. A similar conclusion can be drawn with respect to the volume changes induced by differences in the kinetics of γ′ precipitate dissolution.[18–20] Surface topography is therefore likely related to the heterogeneity of creep behavior between DZ/IDZ. The interdendritic phase exhibits a lower creep resistance than the dendrite core or arms. The heterogeneous distribution of alloying elements and especially W, which is involved in the kinetics of γ′ precipitate dissolution, is most likely the origin of this phenomenon.

Microstructural heterogeneities, such as differences in precipitate size, rafting decay, and misfit differences between the two regions, have already been observed.[4–7,21–24] Furthermore, the differences in precipitate sizes have been observed following standard heat treatments.[25] Nathal and Murakumo reported on the influence of the mean precipitate size on the creep response.[26,27] All of these arguments point to differences in mechanical behavior between both regions, which were never demonstrated experimentally. This "composite character" most likely gives rise to strength redistribution during creep experiments. In this study, the mechanical behavior of this heterogeneous material is attributed to the direction of mechanical loading relative to the microstructural elements composing the material. In

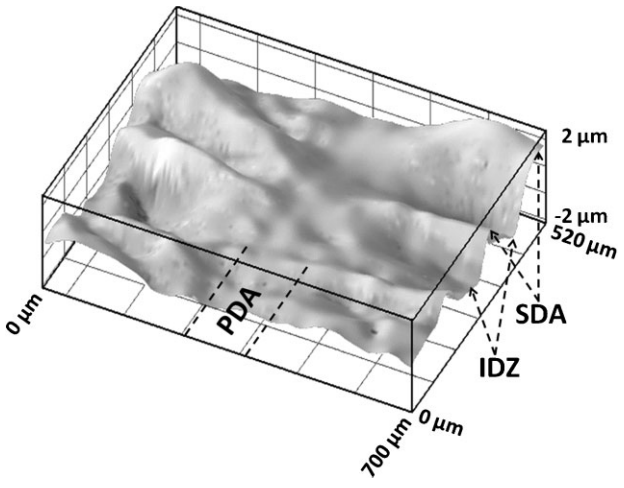

Fig. 5. Optical interferometry analysis.

conclusion, such mechanical heterogeneities may be harmful to the in-service lifetime of thin-walled blades due to the associated size effect, which was taken into account from a mechanical and not an environmental point of view.

High-temperature creep tests were performed on thin specimens (50–200 μm) extracted from a single-crystal superalloy bar. These experiments revealed heterogeneities in creep behavior at a mesoscopic scale, attributed to differences in creep strength between dendrite cores and interdendritic regions. The results singled out the strengthening effect induced by PDA in the superalloy, which therefore behaves as a composite material. The ultrathin specimens were extremely sensitive to foundry defects, intrinsic of the elaboration process and the IDZ. This study demonstrates the need to introduce this mesoscopic scale of heterogeneity to describe the mechanical behavior of Ni-based SX superalloy.

1. Experimental

1.1. Preparation of Ultrathin Tensile Specimens

Creep tensile specimens (length of gauge zone of 20 mm and width of gauge zone of 2 mm) were machined by electric discharged machining (EDM) along the [001] axis of the rod. Two hundred micrometers of material was removed by grinding down to P4000 SiC paper each side and edge of the specimen to avoid any effect of the thermally affected zone due to EDM. A maximal disorientation of 2.1° relative to the [001] crystallographic direction and the loading direction was observed. The lateral faces of the specimens were machined parallel to the SDA. Samples were then thinned taking care of both the parallelism and uniform thickness of the specimens, down to 50–170 $\mu m \pm 2\,\mu m$, i.e., thinner than the period of the dendritic motif. Assuming that the sample thickness does not induce modifications in the MC2 Norton's law parameters, thickness variations lead to a maximal error of ≈30% in the steady-state creep rate.

1.2. Mechanical Test Rig Dedicated for Ultrathin Specimens

Testing ultrathin specimens requires deadweight loading inside the sealed vessel. Specimen heating is performed using a 2-zone halogen lamp furnace. The temperature is measured by two S-type thermocouples welded onto thin Pt sheets located near the gauge zone. A $30\,°C\,min^{-1}$ heating rate was used to reach the experimental temperature of 1100 °C. The strain was calculated based on the relative displacement of the specimen grips by using a contact-less LED/CCD optical micrometer. Creep deformation was assumed to begin once the dwell temperature was reached.

1.3. EPMA Analysis

The chemical homogeneity was quantified using a Cameca SX-50 Electron Probe Microanalyzer (EPMA). The analysis conditions (15 kV, 20 nA) allowed for the evaluation of the chemical composition with an accuracy of approximately 300 ppm. The analysis of each element was calibrated with real standards. Ta and W interactions were considered for quantitative analysis. A dendritic motif was mapped using a square grid of measurements. Each analysed spot of $8\,\mu m^3$ corresponds to about 100 γ′ precipitates, which is large enough to be representative of the material in terms of volumetric fraction.

1.4. Interferometry Analysis

The local topography of the specimen was investigated using a Zygo1000 optical interferometer. The analyzed area, 2.5 mm away from the fracture area, covers $530 \times 700\,\mu m^2$, with an out-of-plane z resolution of 10 nm.

[1] F. I. Versnyder, M. E. Shank, *Mater. Sci. Eng.* **1970**, *6*, 213.
[2] P. Caron, T. Khan, J. L. Raffestin, in. *Euromat' 89* (Eds: H. E. Exner, V. Schumacher), DGM Informationgesellschaft mbH, Aachen **1989**, p. 333.
[3] F. Diologent, P. Caron, T. Almeida, A. Jacques, P. Bastie, *Nucl. Instrum. Methods B* **2003**, *200*, 346.
[4] H. Mughrabi, *Mater. Sci. Technol. Ser.* **2009**, *25*, 191.
[5] U. Bruckner, A. Epishin, T. Link, *Acta Mater.* **1997**, *45*, 5223.
[6] R. Volkl, U. Glatzel, M. Feller-Kniepmeier, *Acta Mater.* **1998**, *46*, 4395.
[7] T. Link, A. Epishin, U. Bruckner, P. Portella, *Acta Mater.* **2000**, *48*, 1981.
[8] R. Hüttner, J. Gabel, U. Glatzel, R. Völkl, *Mater. Sci. Eng. A Struct.* **2009**, *511*, 307.
[9] M. Bensch, E. Fleischmann, C. Konrad, R. Völkl, C. M. F. Rae, U. Glatzel, in. *Superalloys 2012* (Eds: S. Huron, R. C. Reed), Wiley, Warrendale **2012**, p. 387.
[10] A. Srivastava, S. Gopagoni, A. Needleman, V. Seetharaman, A. Staroselsky, R. Banerjee, *Acta Mater.* **2012**, *60*, 5697.
[11] S. Dryepondt, D. Monceau, F. Crabos, E. Andrieu, *Acta Mater.* **2005**, *53*, 4199.
[12] E. Fedorova, D. Monceau, D. Oquab, *Corros. Sci.* **2010**, *52*, 3932.
[13] M. Gungor, *Metall. Mater. Trans. A* **1989**, *20*, 2529.
[14] M. S. A. Karunaratne, D. C. Cox, P. Carter, R. C. Reed, in *Superalloys 2000* (Eds: T. Pollock, R. D. Kissinger), TMS, Warrendale **2000**, p. 263.
[15] E. Caldwell, F. Fela, G. Fuchs, *JOM – J. Miner. Met. Mater. Soc.* **2004**, *56*, 44.
[16] T. Pollock, S. Tin, *J. Propul. Power* **2006**, *22*, 361.
[17] J. B. Le Graverend, J. Cormier, S. Kruch, F. Gallerneau, J. Mendez, *Metall. Mater. Trans. A* **2012**, *43*, 3988.
[18] J. Cormier, X. Milhet, J. Mendez, *J. Mater. Sci.* **2007**, *42*, 7780.
[19] C. Siret, *INPT Thesis*, **2010**, p. 217.
[20] X. Milhet, M. Arnoux, J. Cormier, J. Mendez, C. Tromas, *Mater. Sci. Eng. A Struct.* **2012**, *546*, 139.
[21] R. Volkl, M. Feller-Kniepmeier, U. Glatzel, *Scr. Mater.* **1998**, *38*, 893.

[22] A. Epishin, T. Link, U. Bruckner, P. D. Portella, *Acta Mater.* **2001**, *49*, 4017.
[23] K. Y. Cheng, C. Y. Jo, T. Jin, Z. Q. Hu, *Mater. Des.* **2010**, *31*, 968.
[24] X. Milhet, J. Cormier, M. Arnoux, C. Tromas, in *Creep and Fracture of Engineering Materials and Structures* (Eds: K. Maruyama, F. Abe), The Japan Institute of Metals, Kyoto **2012**.
[25] T. Grosdidier, A. Hazotte, A. Simon, in *High Temperature Materials for Power Engineering 1990* (Eds: E. Bachelet, R. Brunetaud), Kluwer Academic Publishers, Liège **1990**, p. 1271.
[26] M. Nathal, *Metall. Mater. Trans. A* **1987**, *18*, 1961.
[27] T. Murakumo, T. Kobayashi, Y. Koizumi, H. Harada, *Acta Mater.* **2004**, *52*, 3737.